J. Fluid Mech. (1998), *vol.* 358, *pp.* 203–221. Printed in the United Kingdom

Liquid surface in regular *N*-pods

By A. DE LAZZER AND D. LANGBEIN

Center of Applied Space Technology and Microgravity, ZARM, University of Bremen,
Am Fallturm, 28359 Bremen, Germany
e-mail: delazzer@zarm.uni-bremen.de, d.langbein@t-online.de

(Received 18 October 1995 and in revised form 23 April 1997)

The shape of liquid surfaces in regular N-pods in the absence of gravity is considered. A liquid volume in the vertex of a regular N-pod wets the adjacent faces if the sum of the liquid's contact angle γ with the faces and half the dihedral angle α between adjacent faces is smaller than $\pi/2$. A suggestion for why the surface shape in the wedge approaches its cylindrical shape at infinity exponentially is given. The range of this exponential decrease is related to the curvature of the meniscus and the angles α and γ: The decrement of the decrease generally shows a weak dependence on $\alpha+\gamma$, predominantly depending on the liquid volume. Extremely close to the wetting limit, when $\alpha+\gamma$ approaches $\pi/2$, the decrement vanishes. The exponential meniscus shape leads to a similarity relation and allows small relative liquid volumes in polyhedrons to be split up into partial volumes ascribed to the corners and others ascribed to the wedges. The respective relations among volume, curvature, contact angle and corner geometry are obtained by numerical simulation and the limits of applicability are discussed. This greatly simplifies the calculation of liquid surfaces in the limit of small liquid volumes. The results obtained apply to liquid surfaces in a Space environment, e.g. to metallic melts in crucibles and to propellants and other technical fluids in tanks and reservoirs, as well as to liquid surfaces on Earth, e.g. to liquids trapped in polyhedral pores and to liquid foams, provided their characteristic length is sufficiently small compared to the capillary length.

1. Introduction

Since the advent of microgravity research, the shape of liquid surfaces in different containers has received increasing attention. Under weightlessness, the shape of liquid surfaces is no longer determined by gravity pressing the liquid to the bottom, but solely by the liquid volume, the container shape and the liquid's contact angle with the container material. Wetting liquids maximize their wall contact, whereas non-wetting liquids tend to reduce it. Corners provide a stronger wall contact than wedges or even faces, such that wetting liquids pile up there. Nevertheless, corners do not fully dominate wedges: there are situations when the wedges just do not release the liquid and remain filled however strong the sucking forces might be. This effect has long been known in materials sciences. The nucleation energy of a melt in corners and wedges may become negative if the angles between the faces become sufficiently small (Volmer 1939; Pötschke 1980); Gibbs probably was already aware of that. It allows premature nucleation to take place in the wedge.

Among the obvious applications of liquid behaviour in containers with different shape are: on the technical side all questions of liquid transport due to capillary forces, in particular surface tension tanks and heat pipes; on the scientific side all

microgravity experiments in materials sciences, life science and fluid dynamics which involve different fluids; the configuration and drainage of foams made up from polyhedral segments.

Detailed studies on capillary surfaces in domains with wedges and corners have been reported only recently. The advance of Space technology has required a close look at liquid handling under microgravity conditions. In these applications (life science, fuel systems, heat exchange etc.) partially filled containers with edges or corners are in common use. Among the microgravity experiments, materials sciences have played an important role. In the mid 1970s experiments on the solidification of monotectic alloys under microgravity conditions showed that containers with edges and corners may strongly affect the final distribution of the two consolutal phases in the solidified material (Ahlborn & Löhberg 1976). In the meantime, additional microgravity conditions have become available in drop towers, sounding rockets, satellites and Space missions and many more experiments have been flown.

Another promising field of application is the characterization of the wetting of porous structures. Materials exhibiting pores of aspect ratios close to unity can be regarded as structures of coupled polyhedrons of different sizes. If the pores considered are small, the Bond number is also small, and gravity becomes unimportant. Under these assumptions, the results presented in the following can also be applied to porous media. In the limit of low relative filling levels, simple relations characterizing the meniscus curvature can be obtained. These result from using similarity principles and numerical simulation. This may considerably extend studies by Princen on wetting and drainage in fibrous structures (Princen 1969*a*, *b*, 1970) and by Mason & Morrow on the menisci in pores of general tubular shape. Considering the height of rise of liquid menisci in long capillaries of irregular cross-section, they found excellent correspondence between calculated curvatures and respective theoretical maximum meniscus elevation and experimental data obtained on the ground (Mason & Morrow 1984). Additionally, Mason & Morrow (1991) closely examined the menisci in irregular triangular tubes. They also considered the menisci in an isolated wedge of infinite extent and discussed the generalized problem of capillary rise in a capillary of arbitrary cross-section immersed in a liquid reservoir. They could not account for closed capillaries or general vessels containing very small amounts of fluid, where wetting of the bottom has to be considered and menisci partially wetting the bottom but entirely covering the wedges might arise.

In the relevant mathematical literature on liquid surfaces in infinite cylinders (Concus & Finn 1969; Finn 1986 and others), the cross-section of the cylinders is termed the domain and the wedges of the cylinders are termed corners. Since we are dealing with physical three-dimensional containers, we do not adopt that terminology. Instead we keep the physical terminology, i.e. a cube has six faces, eight corners and twelve wedges; each wedge results from the intersection of two faces and its dihedral angle equals the angle between the normals of the respective faces. The geometrical line of intersection of two faces, i.e. the apex of the wedge, is termed the edge.

Let us quite generally consider a wedge k with dihedral angle α_k, which is formed by two faces i and j with contact angles γ_i and γ_j, respectively. For a capillary surface to exhibit a contact line up to the wedge, the normal of the surface must lie on the cone with angle γ_i around the normal of face i and on the cone with angle γ_j around the normal of face j.

Four different situations can occur.

(i) The two cones lie outside each other

$$\gamma_i + \gamma_j < \pi - 2\alpha_k. \tag{1.1}$$

A contact line up to the wedge cannot exist. The liquid fully penetrates into the wedge. In the absence of external forces a stable concave cylindrical meniscus is formed. The concave shape means a capillary underpressure, which sucks the liquid into the wedge.

(ii) The two cones intersect, i.e. a capillary surface up to the wedge exists, if

$$\gamma_i + \gamma_j \geqslant \pi - 2\alpha_k. \tag{1.2}$$

Alternatively in an infinite wedge, an unstable convex meniscus subject to breakage can be found. The wavelength of this breakage under the premises of weightlessness and the absence of other external forces has been calculated by Langbein (1990). Equation (1.2) is subject to the following restrictions:

(iii) The two cones lie inside each other

$$|\gamma_i - \gamma_j| > \pi - 2\alpha_k. \tag{1.3}$$

This is the case of canthotaxis. The contact line extends up to the wedge where it gets pinned for a finite interval, in which the normal of the capillary surface turns from γ_i to $\gamma_j + 2\alpha_k - \pi$.

(iv)
$$\gamma_i + \gamma_j > \pi + 2\alpha_k. \tag{1.4}$$

This is equivalent to $(\pi - \gamma_i) + (\pi - \gamma_j) < \pi - 2\alpha_k$. The cones with the complementary contact angles $(\pi - \gamma_i)$ and $(\pi - \gamma_j)$ do not overlap. The complementary fluid penetrates into the wedge. In the following we will refer to (1.2)–(1.4) in a mutually exclusive sense, i.e. if (1.2) is said to 'hold' then neither (1.3) nor (1.4) will apply.

This behaviour was established mathematically by Concus and Finn (Concus & Finn 1969; Finn 1986). In the mathematical sense the penetration of liquid into a wedge according to condition (1.1) or (1.4) represents a discontinuity: there is no longer a surface over the full cross-section (domain). Physically, the change in pressure when the liquid penetrates into a wedge is not dramatic: in the infinite wedge, pressure and curvature even change continuously from positive to negative values. It will be shown below that the curvature of capillary interfaces in three-dimensional corners changes smoothly, when the adjacent wedges become wetted.

The wetting condition applies to even more general geometries: physical liquid surfaces in three-dimensional corners made up of three faces do exist, if for each of the wedges (1.2) or (1.3) holds. If (1.2) holds and the three cones around the normals of each face intersect, the meniscus forms a spherical cap. The spherical meniscus shape is the only solution of the capillary equation known under this premise. For convex liquid drops in such corners, the uniqueness of the spherical shape has been proven recently (Finn & McCuan 1997). From an engineering point of view, uniqueness of the spherical solution is likely for concave drops in corners, too. Under this premise, it is possible to calculate analytically the volume and surface area of spherical liquid drops in arbitrary tripods (Langbein 1995).

In the following, interfaces wetting all wedges of the respective corner will be considered, i.e. either (1.1) or (1.4) will hold for all wedges. Furthermore and without lack of generality, we restrict our attention to interfaces establishing identical contact angles $\gamma_i = \gamma_j = \gamma$ on all faces of the respective corner.

At large distances from the corner the liquid surface asymptotically assumes the above-mentioned cylindrical shape. Cylindrical surfaces in different wedges connected

by corners assume identical pressure and thus identical radii. It has been concluded from one-dimensional modelling that the evolution of the cylindrical surface in the wedges to the liquid volumes piled up in the corners generally follows an exponential law (Langbein 1994). This allows the splitting of the total liquid volume in polyhedral containers into cylindrical volumes in the wedges and surplus volumes piled up in the corners. Unlike the analytical approach for spherical interfaces confined in corners which is valid only for $N = 3$ where N is the number of wedges, the present considerations on interfaces also wetting the adjacent wedges is valid for any N.

The aims of the present paper are (i) to determine by appropriate numerical calculations the behaviour of a liquid meniscus extending into a wedge and to verify the exponential law obtained analytically, (ii) to verify, whether the analytically derived similarity solutions for liquid menisci extending from a corner into the adjacent edge hold, (iii) to determine numerically the characteristic volumes piled up in the corners and to analyse the curvature of the interface with respect to the contact angle when crossing the wetting limit $\alpha + \gamma = \pi/2$, (iv) to determine the range of applicability of the volume decomposition of liquids wetting the corners and wedges of finite polyhedral containers, and (v) to use the present results for a simplified calculation of the mean curvature of liquid menisci in polyhedrons.

Therefore the present paper recalls in §2 a recent approach to study the shape of liquid menisci extending from a corner into the adjacent edges, giving a more convenient derivation of the respective equations. In §3 we confirm by numerical simulation that the meniscus approaches its final cylindrical shape exponentially. The decrement of this approach can be given analytically. In general, it turns out that for constant liquid volumes the decrement assumes the order of magnitude of the inverse mean curvature for small contact angles, slightly increases with γ and after assuming a maximum value near to the non-wetting region tends to zero for $\alpha + \gamma \approx \pi/2$. We show that liquid menisci with equal contact angles γ enclosing different volumes belong to a family of similarity solutions, which are mutually related by curvature (pressure) and the above exponent. The analytical decomposition of the total liquid volume into cylindrically shaped portions in the wedges and surplus volumes piled up in the corners is demonstrated in §4. In §5 we verify this decomposition by numerical simulation and derive the corresponding scaling factors. This enables us to establish the relation between the total liquid volume and the curvature of the meniscus for different geometries over the whole range of angles $0 \leqslant \alpha+\gamma \leqslant \pi$. The numerical data provide a continuous extension of the analytical relations obtained for non-wetted wedges, $\alpha + \gamma \geqslant \pi/2$ (Langbein 1995), to the region of wetted wedges, $\alpha + \gamma < \pi/2$. The curvature of the meniscus changes smoothly when crossing the wetting limit of the wedges, for interfaces having constant liquid volumes associated with the corners as well as for interfaces enclosing constant total liquid volume. Finally the results are applied to the calculation of liquid menisci in cubes and compared with recent fully numerical calculations (Mittelmann 1993*b*) in §6.

Throughout this paper we deal with ideal static liquid surfaces only. That means that all solid surfaces must be perfectly smooth without any scratches or contamination, i.e. of sticking lines are considered. Additionally, no account is taken of kinetics, i.e. of how the liquid surfaces assume their static shape. Kinetics would include the question of the advancing contact angle, which is generally larger than the static contact angle and due to hysteresis may lead to alternative final surfaces. The dynamic behaviour of liquid menisci close to the critical wetting situation has been studied experimentally in the Bubble, Drop and Particle Unit BDPU during the Spacelab mission IML-2 in July 1994.

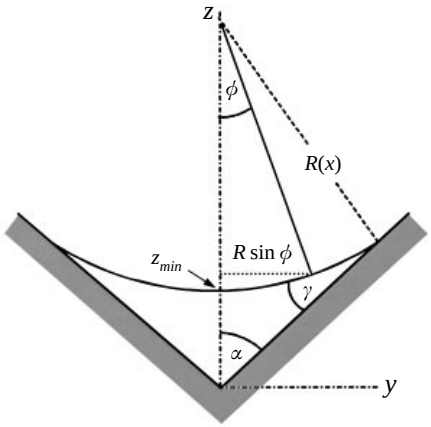

FIGURE 1. Cross-section of a meniscus in a wedge and the coordinates used to obtain the exponential decay of the centre meniscus height.

2. Analytical treatment of liquid surfaces not trapped in corners

Under zero-Bond-number conditions, a liquid volume is trapped in a corner made up of N wedges, if for all wedges k equation (1.2) is valid and the cones with angle γ_i around the normals of the faces i have a common region of intersection. The liquid surface in the corner forms a spherical cap. By introducing appropriate auxiliary sections, the dependence of curvature and surface area on the drop's volume can be calculated analytically (Langbein 1994, 1995).

The analytical description of the meniscus shape in the corner is no longer possible if for any of the wedges $2\alpha_k + \gamma_i + \gamma_j$ is less than π. The liquid volume in the corner penetrates into the respective wedges and approaches a cylindrical shape at infinite distance. To examine the character of this approach, we assume that the liquid surface is already close to the final cylindrical shape. Under this premise, the cross-section of the surface normal to a wedge extending along the positive x-axis is roughly circular with radius $R(x)$

$$y(x,\phi) = R(x)\sin\phi; \quad z(x,\phi) = R(x)\left(\frac{\cos\gamma}{\sin\alpha} - \cos\phi\right), \tag{2.1}$$

where ϕ is the azimuth of the circular section (Langbein 1994) and the contact angles are assumed to be identical $\gamma_i = \gamma_j = \gamma$, see figure 1. The influence of curvature in the wedge direction and the respective change in the maximum azimuth ϕ required for maintaining the correct contact angle are neglected in this one-dimensional model. The Gauss–Laplace formula for the centreline of the surface thus takes the form

$$\frac{1}{R(x)} + \frac{R''(x)\Gamma^2}{(1+\Gamma^4 R'(x)^2)^{3/2}} = \frac{1}{R_{wdg}} \tag{2.2}$$

where

$$\Gamma = \left(\frac{\cos\gamma}{\sin\alpha} - 1\right)^{1/2}. \tag{2.3}$$

R_{wdg} denotes the cylindrical radius in the wedge at an infinite distance from the corner. It is the characteristic length entering the present investigation. Since we exclude external forces, R_{wdg} defines the curvature at any point of the liquid surface.

Let us adopt a more straightforward solution of the Gauss–Laplace equation than given by Langbein (1994). Integration of (2.2) after multiplication with $R'(x)$ and

adjusting the integration constant to $R(x)$ smoothly approaching R_{wdg}, yields

$$\log\left(\frac{R(x)}{R_{wdg}}\right) + \frac{1}{\Gamma^2}\left(1 - \frac{1}{(1+\Gamma^4 R'(x)^2)^{1/2}}\right) = \frac{R(x)-R_{wdg}}{R_{wdg}}. \tag{2.4}$$

Solving (2.4) using a Taylor expansion for $(R(x)-R_{wdg})/R_{wdg} \ll 1$ gives

$$\frac{R(x)-R_{wdg}}{R_{wdg}} = c_1 \exp\left(-\frac{x}{R_{wdg}\Gamma}\right) - \frac{c_1^2}{3}\exp\left(-\frac{2x}{R_{wdg}\Gamma}\right) \pm \dots . \tag{2.5}$$

Thus, under the present assumptions, the meniscus approaches its cylindrical shape at infinity exponentially. If the length of the decrement $R_{wdg}\Gamma$ is small compared to the length of the wedge, it is possible to split up the total liquid volume in a polyhedron into independent contributions ascribed to the wedges and others ascribed to the corners.

R_{wdg} depends mainly on the liquid volume relative to the length of the wedge and on the contact angle γ. Γ is given by the contact angle γ and half the dihedral angle α. It decreases monotonically from a finite value at zero contact angle towards zero in the limiting case. From the numerical simulations presented in §5 it follows that for fixed liquid volumes R_{wdg} is increasing with γ and in the product $R_{wdg}\Gamma$ counteracts the decrease of Γ for nearly any γ except very close to $\alpha+\gamma=\pi/2$. The meniscus therefore approaches its final shape the faster, the smaller γ is, except very close to the non-wetting situation where the decrement tends towards zero. In general, the exponential approach becomes slower with increasing contact angle, since more and more liquid is piled up in the corner and the meniscus height in the wedge decreases.

The exponential behaviour of the meniscus shape is of particular importance for further considerations on the decomposition of the liquid volume: an exponential evolution of the meniscus shape from the corner out into the wedge always leads to a finite surplus volume over the cylindrical volume arising in an isolated wedge.

3. Liquid menisci wetting the edges of a regular tripod

The analytical considerations presented in the preceding section are valid far from the corner and therefore are also applicable to wedges which join at the same corner but have different dihedral angles $2\alpha_k$ and different contact angles γ_i and γ_j, $\gamma_i+\gamma_j+2\alpha_k<\pi$.

For the numerical verification of the results obtained, let us consider liquid menisci in regular tripods as depicted in figure 2. We denote the different angles of a regular tripod as follows: θ_1 is the polar angle between the space diagonal and the face diagonals; θ_2 is the polar angle between the space diagonal and the edges, ζ is the angle between the face diagonals and the edges; i.e. half the angle between two adjacent edges; and α is half the dihedral angle between adjacent faces.

These angles are closely related, see Langbein (1994). In regular N-pods each of them fixes the other three. The Bond number is zero, i.e. no external forces act on the liquid. The meniscus thus assumes a uniform mean curvature H. Without loss of generality we assume equal contact angles γ on all faces of the corner. Far from the corner the meniscus assumes the centre meniscus height z_{wdg}. If the edge is sufficiently long for the meniscus to approach its final cylindrical shape, the centre meniscus height z_{wdg} can be calculated from

$$z_{wdg} = R_{wdg}\left(\frac{\cos\gamma}{\sin\alpha}1\right); \quad R_{wdg} = -\frac{1}{2H}. \tag{3.1}$$

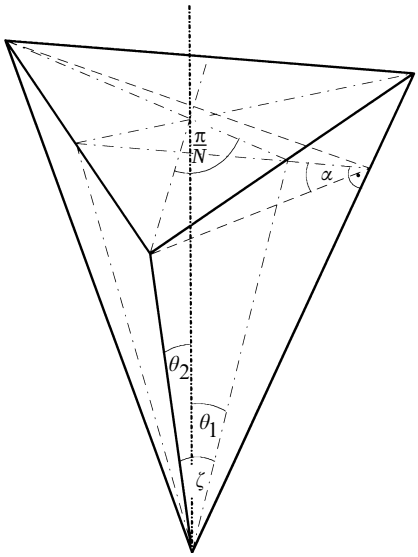

FIGURE 2. Sketch of a regular tripod $N = 3$ defining the angles ζ (angle between the face diagonals and the edges), θ_1 (polar angle between space diagonal and face diagonal), θ_2 (polar angle between space diagonal and edge) and α (half the dihedral angle between two adjacent faces).

Numerical calculations of the capillary surfaces arising in regular tripods have been performed using the SURFACE-EVOLVER, a numerical code developed at The Geometry Center, Minneapolis by K. Brakke (Brakke 1995). The code solves the Laplace equation starting with a given initial configuration towards the nearest minimum of the system's energy. In contrast to other codes that remove the contact line by applying an augmented Laplace equation (Wong, Morris & Radke 1992*a*, *b*), contact lines are preserved in the SURFACE-EVOLVER and contact angles arise due to the energy terms cos γ on the bounding solid surfaces. The same code has been used recently to simulate a variety of different meniscus shapes in unit cubes (Mittelmann & Hornung 1992; Mittelmann 1993*a*, *b*, 1995) and in complex shaped surface tension tanks (Dominick & Tegart 1994).

For the numerical simulation of liquid menisci in tripods with different dihedral angles 2α and contact angles, a tripod with wedges of fixed length has been used. At the end of the wedges, a contact angle of 90° between the meniscus and a fictitious endplane perpendicular to the wedge has been imposed (i.e. the meniscus was assumed to have zero slope along the wedge).

Considering the meniscus shapes formed by identical liquid volumes with different contact angles in a given tripod, the results of the numerical calculations show that the centre meniscus height approaches its minimum value z_{wdg} very fast, see figure 3. The decay of the centre meniscus height in the wedge direction apparently follows an exponential law rather than a power law. Furthermore the range of the decay is considerably shorter for small contact angles, contradicting the analytical tendency of $\Gamma(\alpha, \gamma)$ in (2.3).

To judge whether the decay is indeed exponential, the logarithmic slope of the centre meniscus height $\log(-\mathrm{d}z(x)/\mathrm{d}x)$ is plotted in figure 4 for the rectangular tripod

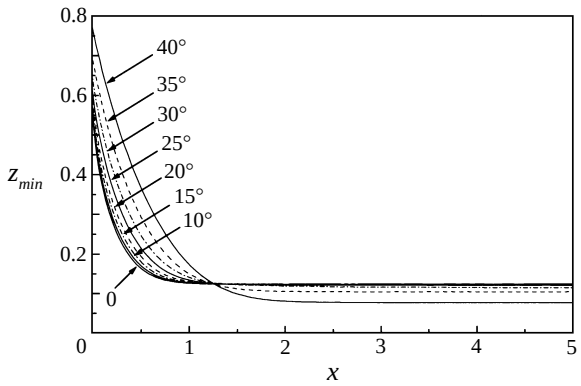

FIGURE 3. Numerically obtained centre meniscus height z_{min} versus the edge coordinate x of a rectangular tripod for different contact angles γ of the liquid (dimensional quantities). The corner of the tripod is located at $x = 0$ and the z-axis corresponds to the face-diagonal opposite to the edge. At $x = 5.0$ the meniscus is forced to form contact angle 90° with a fictitious plane perpendicular to the edge.

and different contact angles. Where the numerical data do not scatter†, the decay definitely tends to become linear in the (dimensional) wedge coordinate x, confirming the exponential behaviour. The graphs for differing contact angles also show that the exponential behaviour develops considerably faster for small contact angles than for large ones. This is due to the meniscus shape becoming more and more spherical close to the corner with increasing contact angle until at $\alpha + \gamma = \pi/2$ the spherical cap is left. Furthermore, the exponential slope is steeper for contact angles close to zero. This can be described in terms of the decrement $R_{wdg}\Gamma$ as shown in figure 5, illuminating the influence of varying curvature on the decrement, as given in (3.1). The increase of R_{wdg} with Γ for a fixed liquid volume counteracts the decrease of Γ. Thus the dimensional decrement R_{wdg} assumes a finite value for zero contact angle, increases slowly with increasing γ and assumes a maximum value rather close to $\alpha + \gamma = \pi/2$. It tends to zero for $\alpha + \gamma$ approaching $\pi/2$, since in that limiting case the cylindrical meniscus in the wedge vanishes, whereas the spherical curvature in the corner remains finite.

4. Similarity of liquid volumes in corners and wedges

The characteristic behaviour of the meniscus protruding from a corner into the adjacent edges, i.e. the exponential approach to a cylindrical shape at infinite distance

† The scattering of the data points when the logarithm decreases below -6 is due to the limited numerical accuracy: in the numerical algorithm, the first and second partial derivatives of the surface shape have to be interpolated from the data available at the nodes of the triangular numerical mesh. The numerical errors arising in this process limit the accuracy of the simulation. Since the iterative scheme of the numerical program used for the present calculations is a minimization of the systems's energy, the contributions of surface area and volume play an important role in the calculations. During their calculations the squared first partial derivatives of the meniscus surface have to be added to unity. The derivatives become very small as the mensicus approaches its final cylindrical shape and thus surface area, volumes and the forces exerted on the corresponding vertices assume erroneous values. The triangular mesh used in the code leading necessarily to a non-uniformly resolved interface together with the non-uniform character of the meniscus' curvature (orthogonal directions of finite and almost zero curvature) is likely to increase this effect. Other errors might arise during the evaluation of the logarithmic decay using finite node to node differences at the appropriate nodes of the mesh.

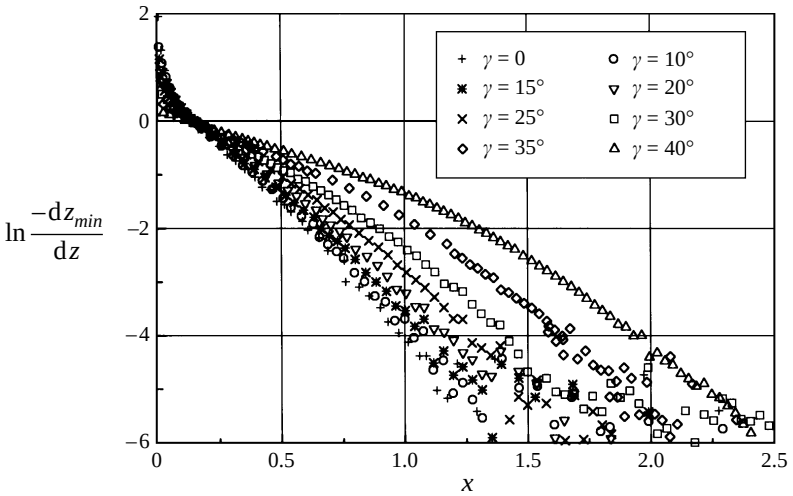

FIGURE 4. Logarithmic decay of the centre meniscus height versus the edge coordinate x of a rectangular tripod for different contact angles γ. For a discussion of the scattering of the results at a logarithmic decay around -6 see the footnote in the text.

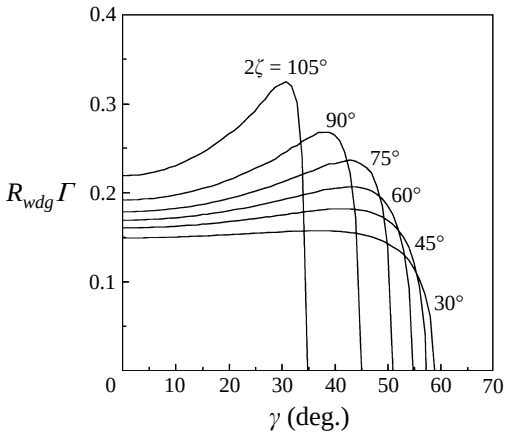

FIGURE 5. Decrement $R_{wdg}\Gamma$ of the meniscus shape versus the contact angle γ for differing dihedral angles 2ζ. Graphs for fixed liquid volume $V = 0.1\pi$ in tripods with edge length $L = 5.0$.

from the corner, suggests a splitting of the total liquid volume into independent portions ascribed to the corners and the wedges (Langbein 1995). The liquid volume can be considered as consisting of portions with cylindrical shape of radius R_{wdg} filling the entire length L of the wedges, thus presenting cylindrical subvolumes. To them one has to add the volume piled up in the corner. Since the meniscus approaches the cylindrical shape in the wedge exponentially, the liquid portion associated with the corner is finite even at infinite wedge length. Therefore, presuming that the filling level is not too large, by cutting off the wedge at a finite distance from the corner only exponentially small errors are introduced. Negligible curvature and slope along the wedge at the wedge end considered is required.

Since the corner volume scales with the third power of the radius R_{wdg} of curvature, whereas the liquid volume in the wedges is proportional to the length of the wedges

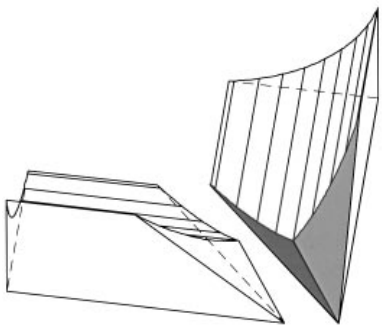

FIGURE 6. Sketch of two out of the three cylindrical menisci meeting in a rectangular tripod. The intersections of the liquid surfaces result in a reduction of the liquid volumes ascribed to the wedges.

and to the cross-section, a relation

$$V = NLV_{wdg}R_{wdg}^2 - NV_{bsc}R_{wdg}^3 + V_{crn}R_{wdg}^3 \tag{4.1}$$

holds. Here, V denotes the total liquid volume, N the number of wedges forming the N-pod, V_{wdg} the specific volume ascribed to the wedge, V_{crn} the specific liquid volume associated with the corner and V_{bsc} an auxiliary term taking into account the intersection of adjacent liquid volumes V_{wdg} in the corner; V_{wdg}, V_{bsc} and V_{crn} are defined geometrically. V_{wdg} can be calculated directly from the cross-section of a cylindrical meniscus in a wedge, yielding for equal contact angles γ

$$V_{wdg} = \frac{\cos\gamma\cos(\alpha+\gamma)}{\sin\alpha} - = \left(\frac{\pi}{2} - \alpha - \gamma\right). \tag{4.2}$$

To obtain V_{bsc}, the cylindrical volumes in the wedges have to be bisected near the corner along the middle planes with the partner wedges. Figure 6 depicts two out of the three cylindrical liquid volumes meeting in the corner of a rectangular tripod; the edge towards the viewer is cut-out and the columns are slightly pulled apart. This yields

$$V_{bsc} = \cot\zeta\left[\frac{1}{3}\frac{\cos\gamma\cos^2(\alpha+\gamma)}{\sin^2\alpha} + \frac{1}{3}\frac{\cos^2\gamma\cos(\alpha)\cos(\alpha+\gamma)}{\sin^2\alpha} + \frac{2}{3}(\cos\gamma - \sin\alpha) - \left(\frac{\pi}{2} - \alpha - \gamma\right)\cos\gamma\cot\alpha\right]. \tag{4.3}$$

In contrast to the specific wedge volume V_{wdg} and the specific bisection volume V_{bsc}, the specific corner volume V_{crn} cannot be obtained analytically but has to be determined by appropriate numerical simulation.

We should point out that the specific quantities introduced (V_{wdg}, V_{bsc} and V_{crn}) have dimension volume per length times area and volume per length^3. Therefore, although they have been introduced as specific 'volumes', they are in fact dimensionless quantities characterizing the meniscus properties in a given geometry.

Equation (4.1) gives the essential similarity relation between the liquid volumes accumulated in a corner and in the adjacent wedges and the curvature of the meniscus. It allows the mean curvature of menisci in corners to be calculated provided that the distortion of the cylindrical meniscus in the wedge by the corner is negligible at the wedge ends. Validity of the similarity relation requires that the meniscus distortion in the corner is integrable and finite. Too large liquid volumes violate (4.1).

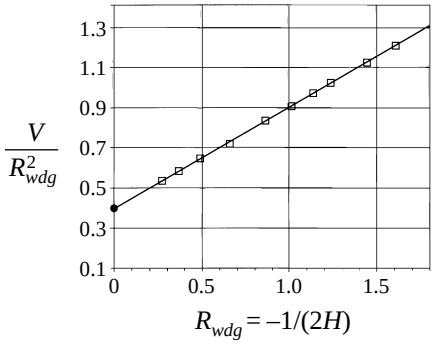

FIGURE 7. V/R_{wdg}^2 versus the meniscus curvature obtained by numerical simulation for different liquid volumes with contact angle $\gamma = 35°$ in a rectangular tripod. R_{wdg} denotes the dimensional curvature of the cylindrical section of the meniscus far away from the corner and H is the mean curvature of the meniscus. Open squares denote the numerical results for relative liquid volumes $V/V_{min} = 1, 2, 4, 8, 16, 24, 32, 40, 60, 80$; the solid line gives the corresponding linear fit ending for $R_{wdg} = 0$ at $3LV_{wdg}$ (solid dot).

In the following section, (4.1) will be verified numerically for the limit of small liquid volumes.

5. The curvature of liquid volumes in regular *N*-pods

5.1. *Numerical verification of the decomposition of the liquid volume*

For convenient checking of the similarity relation (4.1) numerically, we divide it by R_{wdg}^2 yielding

$$\frac{V}{R_{wdg}^2} = NLV_{wdg} + (V_{crn} - NV_{bsc})R_{wdg}. \tag{5.1}$$

For a series of numerical simulations with different liquid volumes, a graph of (5.1) is given in figure 7. V/R_{wdg}^2 clearly shows a linear dependence on R_{wdg} over a volume range of nearly two decades with respect to a suitably chosen minimum liquid volume V_{min} (here, $V_{min} = 0.0025\pi L$). The graph strongly confirms the present approach, since the linear relation holds in the case of the largest liquid volume in spite of significant axial curvature of the meniscus near the wedge end.

The linear behaviour of the numerical results confirms the existence of a specific coefficient $(V_{crn} - NV_{bsc})$ represented by the slope of the graph in figure 7, which does not depend on the total liquid volume. Since V_{bsc} does not depend on the liquid volume either, V_{crn} must behave likewise and can be calculated from the numerical results using (3.1) and (4.1)–(4.3).

The expected analytical relation between the decay of the centre meniscus height and the radius of the cylindrical meniscus far from the corner is given by (2.5). Normalization of the axial coordinate x along the wedge with the decrement $R_{wdg}\Gamma$ gives

$$x* = \frac{x}{R_{wdg}\Gamma} = \frac{x}{R_{wdg}}\left(\frac{\sin\alpha}{\cos\gamma - \sin\alpha}\right)^{1/2}. \tag{5.2}$$

This transformation fits the different meniscus shapes corresponding to figure 7 to a single graph as shown in figure 8 in terms of the logarithmic slope and thus confirms the scale factor of the similarity solutions. Since the slope of the normalized graphs

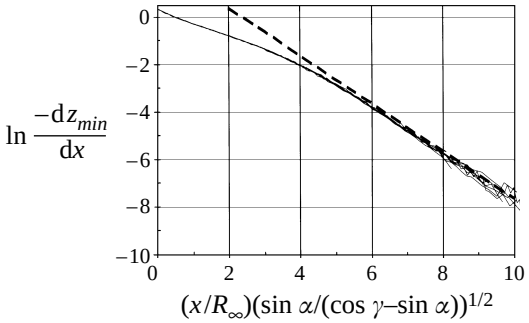

FIGURE 8. Logarithmic decay of the centre meniscus heights versus the normalized axial coordinate of the edge. The normalization proves that the graphs for different liquid volumes ($V/V_{min} = 1$, 2, 4, 8, 16, 24, 32, 60) belong to a family of similarity solutions, the parameter of which is the given scale factor. The slopes of the graphs tend towards -1 (dashed line) for large axial coordinates as predicted by analysis.

given in figure 8 approaches the value of -1 (as represented by the dashed line) for large dimensionless extensions of the wedge $x*$, these results confirm the analytical relation (2.5) for the first-order term of the centre meniscus height. Thus the analytical result yields the scale factor of the meniscus shapes for different liquid volumes and the correct exponent of evolution of the cylindrical meniscus in the wedge as well. The meniscus thereby assumes the predicted exponential behaviour at a dimensionless distance of about 6. The tails of the corner volumes can be considered exponential, if the length of the edge exceeds the decrement $R_{wdg}\Gamma$ by about one order of magnitude.

5.2. *Mean curvature of liquid menisci in tripods with wetted edges*

As discussed in §3, analytical relations for the dependence of the liquid volume on the opening angles of N-pods and the contact angle exist, if the edges are not wetted. Based on the previous results we are now able to give equivalent numerical results for wetted edges. Following the procedure of Langbein (1994), the results will be presented for unit liquid volumes associated with the corners, thus yielding dimensional curvatures.

The mean curvatures for given liquid volumes, corners and wedges are obtained by numerical calculation of the liquid meniscus in the corresponding N-pod. From the numerical results V_{crn} is derived as described in §5.1; the results for different dihedral angles are given in figure 9. It is important to note that, for γ approaching zero, the graphs for V_{crn} assume zero slope for each dihedral angle of the tripod.

To obtain the radius of mean curvature for a unit volume associated with the corner,

$$V_{crn}R_{wdg}^3 = 1 \tag{5.3}$$

has to be solved for $1/R_{wdg} = -2H$. Figure 10 shows twice the mean curvature $2H$ for various tripods and contact angles γ including wetted wedges as well as non-wetted ones. Since the meniscus assumes a concave shape, the mean curvature has been given a negative sign. It is obvious that the results for $\alpha+\gamma < \pi/2$ obtained by the numerical approach provide a continuous extension of the analytical results for $\alpha + \gamma \geqslant \pi/2$, although the interface configuration behaves discontinuously.

It is important to note that for all angles 2ζ of the edges the curvature approaches its value for the contact angle $\gamma = 0$ with zero slope as is anticipated by the behaviour

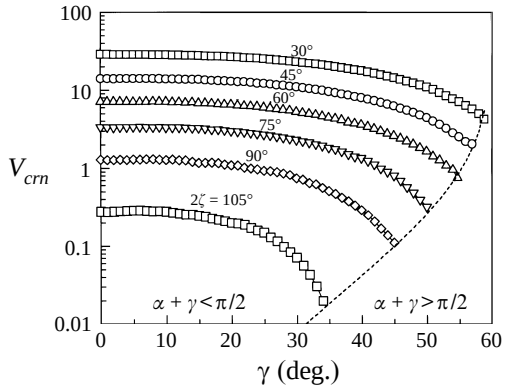

FIGURE 9. Numerically obtained specific corner volumes V_{crn} for regular tripods with dihedral angles 2ζ versus the contact angle γ.

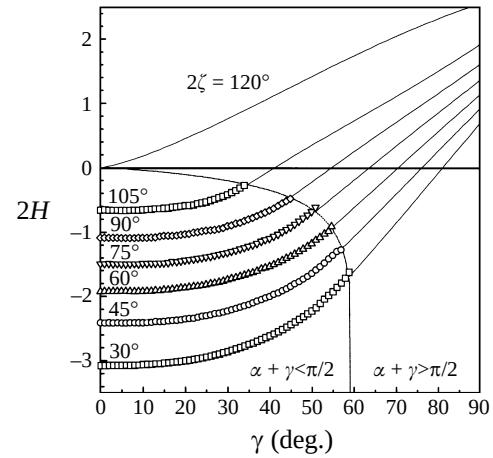

FIGURE 10. Twice the mean curvature $2H$ of a drop with unit corner volume in regular tripods of dihedral angles 2ζ versus the contact angle γ of the liquid. The numerical simulations yield a continuous extension of the analytic results for $\alpha + \gamma \geqslant \pi/2$ (Langbein 1994, 1995) into the region of $\alpha + \gamma < \pi/2$.

of V_{crn} as given in figure 9. This strengthens the theoretical approach (4.1), since for V_{wdg} and V_{bsc} we have

$$\lim_{\gamma\to 0} \frac{\partial V_{wdg}}{\partial \gamma} = 0 \quad \text{and} \quad \lim_{\gamma\to 0} \frac{\partial V_{bsc}}{\partial \gamma} = 0 \tag{5.4}$$

and the exponent of the exponential decay assumes zero slope, too:

$$\lim_{\gamma\to 0} \frac{\partial}{\partial \gamma}\left(-\frac{x}{R_{wdg}\Gamma}\right) = \lim_{\gamma\to 0} \frac{x}{2R_{wdg}} \Gamma^{-3} \frac{\sin\gamma}{\sin\alpha} = 0. \tag{5.5}$$

Since all relevant analytic parameters approach $\gamma = 0$ with zero slope as well as the numerically derived specific corner volumes, the calculated curvature of the meniscus must behave likewise.

With figure 10 we have shown that the mean curvature for capillary interfaces of unit corner volume (i.e. for $\alpha+\gamma \geqslant \pi/2$ for liquid drops of unit volume and $\alpha+\gamma < \pi/2$ for unit volumes associated with the corners) changes continuously when the wetting

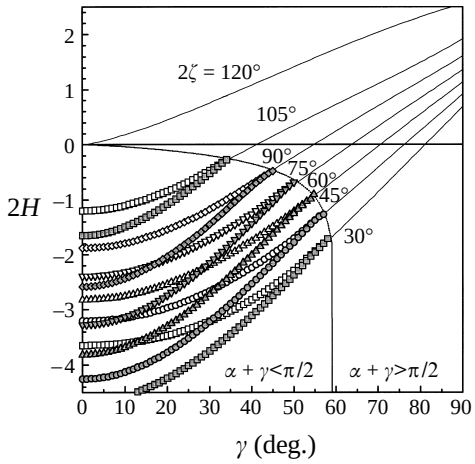

FIGURE 11. Twice the mean curvature $2H$ of a drop with unit total volume in regular tripods of dihedral angles 2ζ versus the contact angle γ of the liquid: graphs for wedge lengths of 5 units (open symbols) and 10 units (shaded symbols). Although the shapes of the interface change discontinuously when the wedges become wetted, the curvature changes continuously.

limit of the wedges is reached. An important result of the present considerations is that the same behaviour can be observed when the total liquid volume is considered. In this case the influence of the length of the wedges taken into account cannot be neglected, since for constant total volume the radius of curvature of the interface will vanish (the curvature thus will diverge) when the length of the wedges tends towards infinity. Once more, interfaces of unit volume – this time of unit total volume – will be considered. The radius of curvature of the interface thus can be obtained by solving

$$(V_{crn} - NV_{bsc})R_{wdg}^3 + NLV_{wdg}R_{wdg}^2 = 1 \tag{5.6}$$

for R_{wdg}. The corresponding mean curvature for the interfaces of unit total volume in regular tripods are plotted in figure 11. For $\alpha + \gamma \geqslant \pi/2$, the graphs naturally coincide with those from figure 10. For $\alpha + \gamma < \pi/2$ open and shaded symbols denote wedges extending 5 units and 10 units, respectively. The graphs show that also in terms of the total liquid volume the curvature of the interface smoothly passes the wetting limit of the wedges, although the characteristic shape of the interface shows a discontinuous behaviour. This emerges from the characteristic behaviour of the specific wedge volume V_{wdg}, which approaches zero with zero slope when $\alpha+\gamma$ approaches $\pi/2$. Likewise the liquid volume associated with the wedge vanishes, overcoming the influence of the length of the wedge (which might even be infinite) allowing a finite radius of curvature of the interface to be formed. The difference between the behaviour of the mathematical problem (discontinuous) and the curvature of the respective interfaces (continuous) is of basic physical interest: since physical surfaces show a smooth behaviour when wetting conditions are changed, the pressure within the liquid likewise varies smoothly.

5.3. *Menisci in wedges joining neighbouring corners*

The previous considerations have been based on the assumption that the dimensionless extent of the wedge $L/R_{wdg}\Gamma$ considerably exceeds unity. The boundary condition set at the end of the wedges was zero slope of the meniscus along the wedge. No meniscus deformation at this far end of the wedge has been considered, although

wedges of finite length L naturally connect corners with differing geometry, but often with equal wetting conditions. For what follows let us recall that the one-dimensional model according to (2.2) accounts for the axial curvature simply by adapting the radius $R(x)$, i.e. the radius or curvature perpendicular to the wedge.

The range of applicability of the similarity solutions nevertheless allows for a certain overlap of volumes in opposite corners. If a wedge joining two corners is sufficiently long, the meniscus arising is approximately the underlying wedge meniscus plus a linear superposition of the two corner volumes extending out into the wedge. The one-dimensional model yields a favourable compensation of errors when the liquid volumes ascribed to opposite corners are cut-off in the middle of wedges. Let us mention in this context the additivity of curvatures and slopes: the curvatures add up, whereas the slopes cancel due to their opposite sign.

The similarity solution stays valid as long as the meniscus shape in the middle of the wedge is well within the regime of exponential decrease and the slopes of the isolated corner volumes are sufficiently small not to violate the one-dimensional approach of (2.2). The similarity solution breaks down when the isolated slopes of the corner volumes in the middle of the wedge cease to follow the exponential decrease. In this case, the influence of the liquid volumes in the tails of the corner volumes on the overall curvature do not mutually cancel any more and the contact angle boundary condition has a relevant influence on the meniscus shape. Both effects change the overall meniscus curvature of the respective opposite corner volume, thus the similarity solution lacks validity.

6. The applicability of the present approach

To check the applicability of the present approach, the numerical calculations by Mittelmann (1993*b*) on the meniscus of a liquid with contact angle $\gamma = 40^\circ$ in a unit cube are compared with the present results. To this end (4.1) is adapted to a unit cube. The wedges of the cube are divided into two halves, each being associated with the adjacent corner. Now on applying (4.1) to each of the eight corners, the total liquid volume within the cube is obtained. An equivalent procedure can be applied to any polyhedral container.

Building the unit cube from eight rectangular tripods $N = 3$ with the length $L = 1/2$ and using

$$2H = \frac{\Delta p}{\sigma} = -\frac{1}{R_{wdg}} \tag{6.1}$$

one obtains from (4.1)

$$V = 8\left\{NLV_{wdg}\frac{1}{|2H|^2} - NV_{bsc}\frac{1}{|2H|^3} + V_{crn}\frac{1}{|2H|^3}\right\}. \tag{6.2}$$

V_{wdg} can be calculated according to (4.2), V_{bsc} from (4.3) and V_{crn} results from numerical simulation as summarized in figure 9; the mean curvature H of the concave meniscus is assumed to have negative sign. The result is given in figure 12 in terms of (5.1), depicting the dependence of twice the mean curvature, $2H$, squared times the liquid volume on the radius of curvature $-1/(2H)$ for both approaches. For radii of curvature up to about 0.33 and liquid volumes up to 0.1 (i.e. up to a filling level of 10%), the results obtained by the present approach fit Mittelmann's calculations with a maximum deviation of the mean curvature $2H$ of $\epsilon < 4\%$ with respect to a given

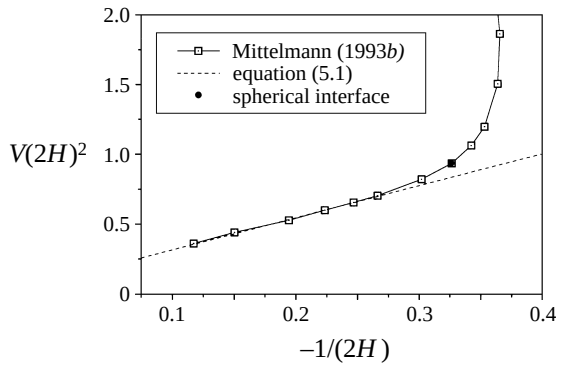

FIGURE 12. Comparison of $V(2H)^2$ obtained by the present approach using (5.1) and by numerical calculations (Mittelmann 1993*b*) versus the inverse mean curvature considering a liquid meniscus wetting the edges ($\gamma = 40°$) of a unit cube.

liquid volume. At radii of curvature below 0.27 the maximum deviation diminishes by one order of magnitude, $\epsilon < 0.4\%$.

This agreement is better than expected, since the sum a+g is rather large but not very close to $\pi/2$, and thus the decrement $R_{wdg}\Gamma$ of the corner menisci is close to its maximum value (compare figure 5). Furthermore it has to be taken into account that the meniscus for $V = 0.1$ is almost spherical, i.e. it does not fulfil the requirements of $R_{wdg}\Gamma \ll L$ and the axial curvature of the meniscus at the end of the wedge being negligible.

Furthermore, figure 12 shows that no contributions of order $1/(2H)^4$ arise in (4.1). This once more confirms the exponential evolution of the meniscus shape. If in the middle of the wedges the fading out of the corner menisci fails to follow the exponential behaviour, significant and exponentially growing deviations from (4.1) and (5.1) arise.

On the other hand, Mittelmann's results are obtained numerically, too. To judge their reliability we consider the particular situation when the liquid surface in a cube assumes a spherical shape. In this particular configuration we obtain

$$R_{sph}\cos\gamma = \tfrac{1}{2}; \quad 2H = -4\cos\gamma \approx -3.064178 \tag{6.3}$$

and

$$V = 1 - \frac{4\pi}{3}R_{sph}^3 + 6\pi R_{sph}^3\left(\tfrac{2}{3} - \cos\gamma + \tfrac{1}{3}\cos^3\gamma\right) \approx 0.099756. \tag{6.4}$$

This proves Mittelmann's result to agree well with the exact value. With the present method yielding an error of $\epsilon < 4\%$ for the spherical meniscus, it can be applied for rather high filling levels, as a view of the resulting meniscus shape (figure 13) clearly shows. The corner meniscus has not faded away at half the length of the wedges, neither is the axial curvature of the meniscus negligible there. In view of the fact that it considers isolated corners with half the adjacent wedges, the error involved in the present approach is strikingly small even in the case of the spherical meniscus.

This strengthens the validation of the superposition of the menisci arising in a wedge joining two corners of similar wetting conditions. In the case of the spherical meniscus with contact angle $\gamma = 40°$ in the unit cube, we obtain for the decrement

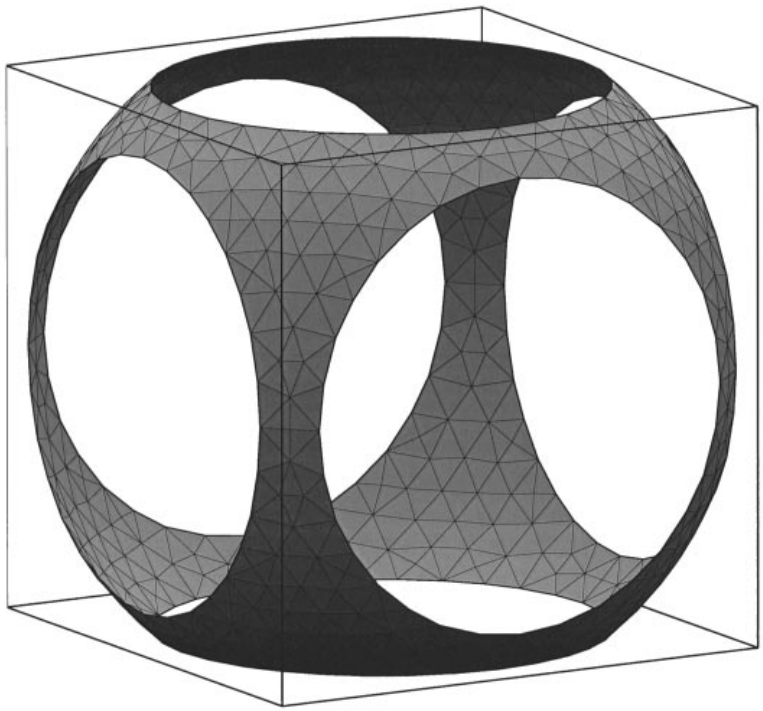

FIGURE 13. Almost spherical meniscus in the unit cube associated to a normalized liquid volume of 0.1, i.e. a filling level of 10%. With the present approach, the mean curvature of this configuration can be determined with an error level below 4%. Thus, the present approach, although based on the assumption that the corner volumes have largely faded away at the end of the wedge, obviously is valid up to comparatively large amounts of liquid and to comparatively small extents of the wedges.

$R_{wdg}\Gamma$ of the corner meniscus as

$$R_{wdg}\Gamma = \frac{1}{4\cos\gamma}\left(\frac{\cos\gamma}{\sin\alpha} - 1\right)^{1/2} \approx 0.09422. \tag{6.5}$$

This is about one fifth of the length L of the wedge attributed to each of the corners. Comparing with the logarithmic slope of the interface as depicted in figure 8 (which, of course, is for a slightly smaller contact angle $\gamma = 35°$), this coincides well with the minimum wedge length required for the slope of the interface to begin to follow the exponential behaviour. The range of applicability of the similarity solutions to menisci in wedges joining corners thus extends to decrements $R_{wdg}\Gamma$ about one order of magnitude lower than the wedge length.

7. Conclusions and prospects

The free liquid surface arising in a corner when the fluid wets the adjacent wedges exhibits an exponential decay from the corner to the wedge. The exponential scaling between different volumes is given analytically. Numerical simulations confirm the exponential behaviour and show that far from the corner the logarithm of the normalized slope of the centre meniscus height is in accordance with the analytical results. The analytical scaling correctly describes the meniscus slope far from the

corner and also gives the scaling between the meniscus shapes arising for different liquid volumes.

The present results show that in the case of wetted wedges a similarity relation between the mean curvature of the meniscus and the geometric situation is valid in the limit of sufficiently small liquid volumes. The similarity solution is based on a decomposition of the liquid volume into portions associated with the corner, the wedges and the intersection of the wedge volumes at the corner. The subvolumes are characterized by specific dimensionless quantities depending merely on corner geometry and boundary data. Although the specific corner volumes cannot be obtained without numerical effort, the present approach has the advantage that for a given geometry the characteristic corner volume has to be determined only once. For determination of specific parameters of an interface configuration, like the dependence of curvature on volume, the present technique thus effectively serves to replace numerical simulation in the limit of small volumes and likewise allows very convenient calculations of the pressure or the mean curvature of menisci in arrays of wedges and corners.

An important result of the present investigations is that the curvature of an interface in a corner changes smoothly when crossing the wetting limit of the adjacent wedges, although the mathematical problem represents a discontinuity. Thus technical fluids initially confined within a corner show a smooth change in pressure/curvature even if finally the wedges become wetted when wetting conditions change, e.g. due to chemical processes within the fluid or the wall (surface ageing), due to electrical fields or due to the addition of surfactants.

The present approach can be extended to more general polyhedral configurations than the examples given above without major numerical effort. It can be applied to any scarcely filled closed container or capillary, thereby significantly extending existing relations on shape, curvature and volume of liquid menisci in long capillaries. Furthermore it allows modelling of foams or porous structures as coupled clusters of polyhedrons filled with low liquid volumes. Within the cluster, all coupled menisci have identical internal pressure, independent of the contact angle. Concerning porous media, a simulation of materials consisting of pores of different shapes and volumes becomes possible.

The authors wish to thank Professor H. D. Mittelmann, Arizona State University, for providing the data of his numerical calculations. Furthermore, we are much indebted to the referees of JFM for their helpful remarks and suggestions. This work was supported by the Deutsche Agentur für Raumfahrtangelegenheiten, DARA, under contract number 50 WM 9432.

REFERENCES

Ahlborn, H. & Löhberg, K. 1976 Ergebnisse von Raketenversuchen zur Entmischung flüssiger Aluminium-Indium Legierungen ("SOLUOG"). *Statusseminar zur Spacelab-Nutzung, BMFT Paper* 12.1.

Brakke, K. 1995 *SURFACE-EVOLVER Manual, Version 1.98*, The Geometry Center, Minneapolis.

Concus, P. & Finn, R. 1969 On the behaviour of a capillary surface in a wedge. *Proc. Natl Acad. Sci.* **63**, 292–299.

Concus, P. & Finn, R. 1996 Capillary wedges revisited. *SIAM J. Math. Anal.* **27**, 56–69.

Dominick, S. & Tegart, J. 1994 Orbital test results of a vaned liquid acquisition device. *AIAA Paper* 94-3027.

Finn, R. 1986 *Equilibrium Capillary Surfaces*. Grundlehren der Mathematischen Wissenschaften, vol. 284. Springer.

Finn, R. & McCuan, J. 1997 Vertex theorems for capillary drops on support planes. *MSRI* 1997-077. Mathematical Sciences Research Institute, Berkeley, C.A.

Langbein, D. 1990 The shape and stability of liquid menisci at solid edges. *J. Fluid Mech.* **213**, 251–265.

Langbein, D. 1994 Liquid surfaces in polyhedral containers. In *Proc. Intl Conf. on Advances in Geometric Analysis and Continuum Mechanics* (ed. P. Concus & K. Lancaster), pp. 168–173. International Press, Cambridge.

Langbein, D. 1995 Liquid surfaces in polyhedral containers. *Microgravity Sci. Technol.* **8**, 148–154.

Mason, G. & Morrow, N. R. 1984 Meniscus curvatures in capillaries of uniform cross-section. *J. Chem. Soc., Faraday Trans.* I **80**, 2375–2393.

Mason, G. & Morrow, N. R. 1991 Capillary behaviour of a perfectly wetting liquid in irregular triangular tubes. *J. Colloid Interface Sci.* **141**, 262–274.

Mittelmann, H. D. 1993*a* Symmetric capillary surfaces in a cube. *Maths and Computers in Simulation* **35**, 139–152.

Mittelmann, H. D. 1993*b* Symmetric capillary surfaces in a cube; Part 2: Near the limit angle. *Lectures Appl. Maths* **29**, 339–361.

Mittelmann, H. D. 1995 Symmetric capillary surfaces in a cube; Part 3: More exotic surfaces, gravity. In *Advances in Geometry Analysis and Continuum Mechanics* (ed. P. Concus & K. Lancaster), pp. 199–208. International Press, Boston.

Mittelmann, H. D. & Hornung, U. 1992 Symmetric capillary surfaces in a cube. *LBL-31850.* Lawrence Berkeley Laboratory.

Pötschke, J. 1980 Die unberuhigte Erstarrung von Aluminium, Silber, Kupfer und Stahl. *Z. Phys. Chem. Neue Folge* **123**, 199–218.

Princen, H. M. 1969*a* Capillary phenomena in assemblies of parallel cylinders I: Capillary rise between two cylinders. *J. Colloid Interface Sci.* **30**, 69–75.

Princen, H. M. 1969*b* Capillary phenomena in assemblies of parallel cylinders II: Capillary rise in systems with more than two cylinders. *J. Colloid Interface Sci.* **30**, 259–371.

Princen, H. M. 1970 Capillary phenomena in assemblies of parallel cylinders III: Liquid columns between horizontal parallel cylinders. *J. Colloid Interface Sci.* **34**, 171–184.

Volmer, M. 1939 Kinetik der Phasenbildung. In *Die Chemische Reaktion Band IV* (ed. K.F. Bonhoeffer), pp. 1–220. Theodor Steinkopff, Leipzig.

Wong, H., Morris, S. & Radtke, C. J. 1992*a* Two-dimensional menisci in nonaxissymmetric capillaries. *J. Colloid Interface Sci.* **148**, 284–287.

Wong, H., Morris, S. & Radtke, C. J. 1992*b* Three-dimensional menisci in polygonal capillaries. *J. Colloid Interface Sci.* **148**, 317–336.